E≋RS

Synthesis of SrTiO₃:Al, Pr phosphors from a complex precursor polymer and their luminescent properties

Joung Kyu Park [a],*, Hojin Ryu [a], Hee Dong Park [a], Se-Young Choi [b]

[a]*Advanced Materials Division, Korea Research Institute of Chemical Technology, Taejon 305-600, South Korea*
[b]*Department of Ceramic Engineering, Yonsei University, Seoul 120-749, South Korea*

Abstract

Red emitting Pr^{3+}, Al^{3+} doped $SrTiO_3$ phosphor was synthesized by a polymeric complex method using metallic nitrates, ethylene glycol and citric acid. $SrTiO_3$ phosphor powder with a large surface area, small particle size and low agglomeration was formed at a low temperature of 600°C. Different particle growth tendency was also observed both above and below 900°C. The luminescent properties of $SrTiO_3$:Al, Pr phosphor were investigated by photoluminescence. Under 359 nm excitation, $SrTiO_3$:Al, Pr phosphor exhibited a strong red emission, peaking at about 620 nm. The intensity of the excitation spectra was enhanced by the addition of Al^{3+} ions. The luminescence mechanism may be related to the interaction between Pr^{3+} and Al^{3+} ions. Al^{3+} ions absorb the exciting radiation, and this absorbed energy is transferred to the Pr^{3+} ions and then emitted from the Pr^{3+} ions. © 2001 Published by Elsevier Science Ltd. All rights reserved.

Keywords: Luminescence; Phosphors; Powders-chemical preparation; $SrTiO_3$–Al,Pr

1. Introduction

The performance of display devices depends on luminescent materials known as phosphors, which generate visible light and color. Phosphors emit visible light when exposed to various energy sources such as photons, electrons, electric fields or plasma. Most phosphors consist of a host material and an activator. The activator must be added in carefully controlled quantities and substitute at the proper cation sites in the host lattice. In addition, phosphors must have narrow size distribution, non-agglomeration and spherical morphology for good luminescent properties.[1] Vogel et al.[2] reported that the intrinsic properties of a phosphor depend on particle size and size distribution. In general, smaller particle size and narrower particle size distribution of the phosphor produce higher luminescent properties.[3]

Conventional solid state methods usually produce agglomerated particles of irregular shapes and wide size distribution. In this regard, improved synthesis methods are of current interest. The main objective of the present investigation is to produce a red emitting $SrTiO_3$:Al, Pr phosphor, for application in field emission displays (FEDs). Chemical synthesis based on polyesters obtained from citrates was developed by Pechini.[4] This process has been applied to the synthesis of over 100 different oxides including a number of titanates, zirconates and niobates. The polymeric precursor method has been successfully used to synthesize exact stoichiometric compounds with fine particles and low agglomeration.[5] In this study, polymeric precursor experiments were conducted to synthesize $SrTiO_3$ phosphors with $(Al^{3+} + Pr^{3+})$ dopants. Strontium titanate has a perovskite type structure of general formula ABO_3, which has a primitive cubic unit cell. Each oxygen has two titaniums as its nearest cationic neighbors, as well as four strontium atoms, coplanar with the oxygen.

In conventional phosphor materials, exciting radiation is directly absorbed by the activator. However, $SrTiO_3$:Al, Pr red phosphor is more complicated; in this phosphor, the activator, which emits the red color, is the Pr^{3+} ion. But the exciting radiation is not absorbed directly by the activator.[6] Consequently, we added an additional ion (Al^{3+}) to the host lattice. This ion may

---

* Corresponding author.
E-mail address: parkjk@pado.krict.re.kr (J.K. Park).

absorb the exciting radiation, which may be transferred to the activator and then emitted from the activator. Praseodymium ions are assumed to prefer octahedral sites, so the Pr^{3+} ions must substitute for the octahedrally coordinated Sr^{2+} ions and emit the red emission from the $^1D_2 \rightarrow {}^3H_4$ transitions. In this study, red emitting $SrTiO_3$:Al, Pr phosphor with the general formula $Sr_{1-x}Pr_xTi_{1-y}Al_yO_3$ was synthesized using the polymeric complex method and the luminescent properties were investigated.

2. Experimental procedure

2.1. Synthesis

The starting materials were $Sr(NO_3)_2$ (99.9%), titanium isopropoxide (99.999%), $Al(NO_3)_3 \cdot 9H_2O$ (99.999%) and $Pr(NO_3)_3 \cdot 6H_2O$ (High Purity Chemical Laboratory Co. Ltd, 99.9%). To prepare appropriate solutions, titanium isopropoxide (0.02 mol), $Sr(NO_3)_2$(0.02 mol) and $Al(NO_3)_3 \cdot 9H_2O$ (0.02 mol) were dissolved into 1.2 mol of ethylene glycole; 0.8 mol of citric acid was then added to this solution, followed by the addition of the stoichiometric amount of $Pr(NO_3) \cdot 6H_2O$. This solution was stirred while being heated at 120°C for water elimination, until a transparent solution was obtained. This solution was reheated to 200°C to initiate the condensation reaction so that a viscous polymeric resin could be obtained. This resin was treated at 350°C to form a charcoal-like porous foam. This foam was milled and then calcined at several different combinations of temperature and duration.

2.2. Characterization

The polymeric resin was analyzed using thermogravimetric analysis (TGA) (Universal V1.8 M TA Instruments) in air up to 1400°C with a heating rate of 10°C/min. The powders calcined at different temperatures were characterized by X-ray diffraction analysis (RIGAKU Inc.) using Cu K_α radiation. We calculated the crystallite sizes using the diffraction peak of the (110) $SrTiO_3$ plane using the Scherrer equation.[7] Characterization of the polymeric resins for different calcination temperatures was performed with FT-IR (FTS-165) spectroscopy measurements. The effect of calcination temperature on the specific surface area of powders was studied using a nitrogen adsorption/desorption surface area analyzer (Micromeritics Int. Corp). Further a BET (Brunauer-Emmett-Teller) type was used to determine surface area from adsorption curves. Photoluminescence spectra were obtained using a Perkin–Elmer LS-50 photoluminescence spectrometer with a Xenon lamp.

3. Results and discussion

3.1. Characterization of polymeric precursor

The TGA curves for the polymeric precursor are illustrated in Fig. 1. The first weight loss (between 80 and 120°C) resulted from the removal of water in the sample. Further large weight loss can be observed between 320 and 600°C. It can be presumed that the heat treatment in this range breaks all the ethylene glycol/citric acid polyester chains due to combustion of the dehydrated polymeric precursor. The DTA-trace shows broad exotherms between 300 and 600°C; no other significant change appears above these temperatures. This means that at 600°C the resin combustion is almost complete and crystallization of the $SrTiO_3$ has occurred.

3.2. Phase formation and particle size analysis

Fig. 2 shows the XRD patterns of the phosphors obtained after calcining the polymeric precursor for 6 h at different temperatures. After calcination at 600°C, the crystalline $SrTiO_3$ and minor amounts of $SrCO_3$ have formed. With further increasing calcination temperature, the crystallinity of $SrTiO_3$ improves and the secondary phase $SrCO_3$ gradually disappears.

Fig. 3 shows the evolution of the relative crystallinity for the powders calcined at 800°C for several hours. The increase of the crystallinity of the perovskite $SrTiO_3$ phase with calcination time is observed in this figure. These results show that the polymeric precursor method needs long duration time to obtain high crystallinity.

Fig. 4 shows the infrared spectra of the same samples. The peak at 1719 cm^{-1} is due to the C=O stretching mode for ester groups (R-COO-R).[8] These groups are formed during the polyesterification reaction between ethylene glycol and citrates. The peaks at 1568 and 1454 cm^{-1} are due to cation coordination by carboxylic groups in the form of a bidentate complex. After heat treatment at 600°C or higher, the peak at 1719 cm^{-1} disappears and an absorption peak at 568 cm^{-1} characteristic for an octahedrally coordinated[9] Ti–O stretching mode is observed. Furthermore, a strong peak at 1454 cm^{-1} related to the carbonate group of $SrCO_3$ is present after calcination at 600, 800, and 1000°C, but almost disappears after calcination at 1200°C.

In Fig. 5 the logarithm of the mean particle size is plotted versus the (inverse) calcination temperature. Mean particle size (D_{BET}) was calculated from experimentally observed BET surface area data (S_{BET}) using

$$D_{BET} = \frac{6}{\rho_T S_{BET}}$$

where ρ_T is the theoretical density. As indicated by the solid line, a change in the slope can be clearly observed
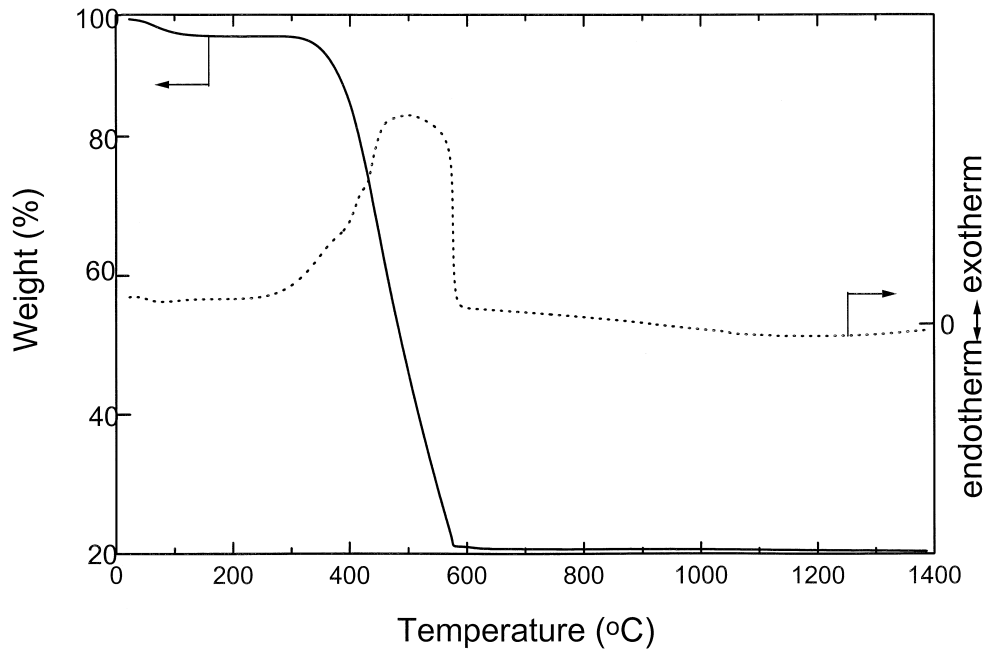
Fig. 1. Thermogravimetric analysis (TGA) and differential thermal analysis (DTA) of polymeric precursor performed in the 20–1400°C temperature range with heating rate of 10°C/min.
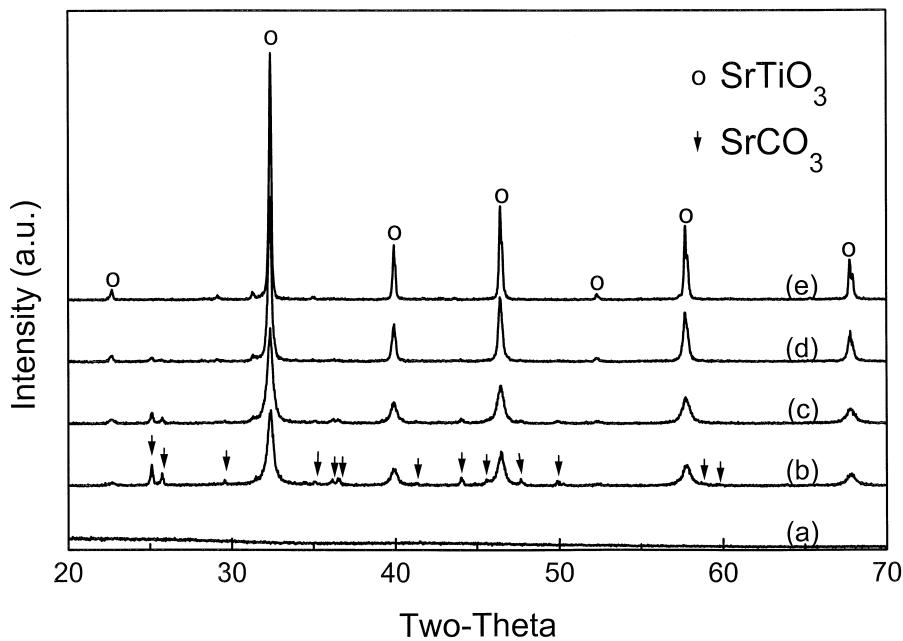

Fig. 2. X-ray diffraction patterns of SrTiO$_3$:Al, Pr phosphors calcinated with different temperatures: (a) 350°C, (b) 600°C, (c) 800°C, (d) 1000°C, and (e) 1200°C.

at 900°C. Fig. 6 shows the relation between particle size (*D*) and calcination time (*t*) at 800°C. Using the model for isothermal grain growth of Gülgün et al.,[10] a growth kinetic exponent of 3 is obtained for the slope. Combining this value and the value for the slope of the solid line for *T* < 900°C in Fig. 5, the activation energy for particle growth (E_a) below 900°C is calculated to be 59 KJ/mol. For temperatures above 900°C, the growth kinetic exponent is considered to be 2,[11,12] an activation

energy of about 168 KJ/mol is obtained. These results indicate a low activation energy process such as grain boundary or surface diffusion dominating particle growth at temperatures below 900°C, and a process with higher activation energy such as lattice diffusion occurring at temperatures above 900°C. This mechanism is similar to that which was proposed by Greskovitch and Lay to explain particle coarsening of alumina in porous materials.[13] The above-mentioned experimental
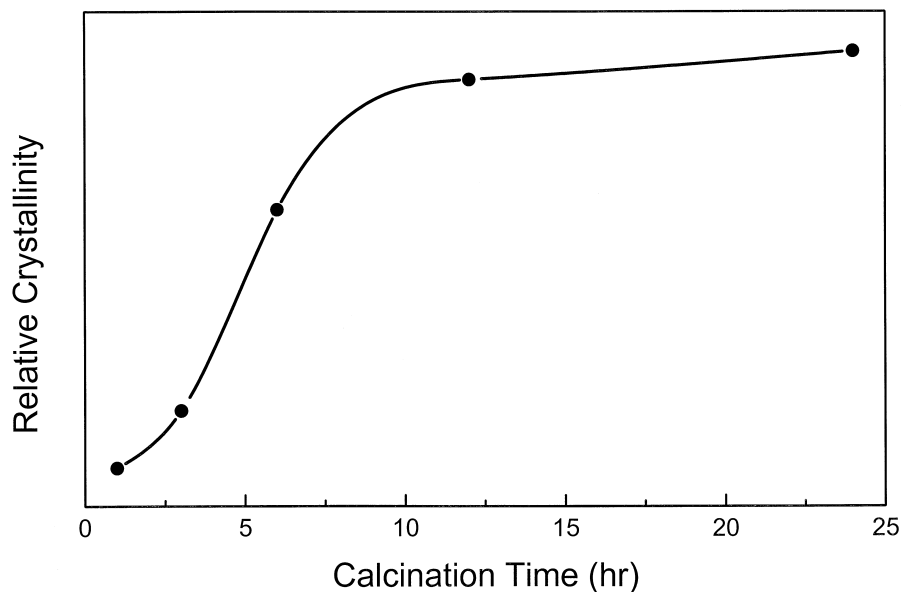
Fig. 3. Crystallinity of SrTiO$_3$:Al, Pr phosphors as a function of duration time.
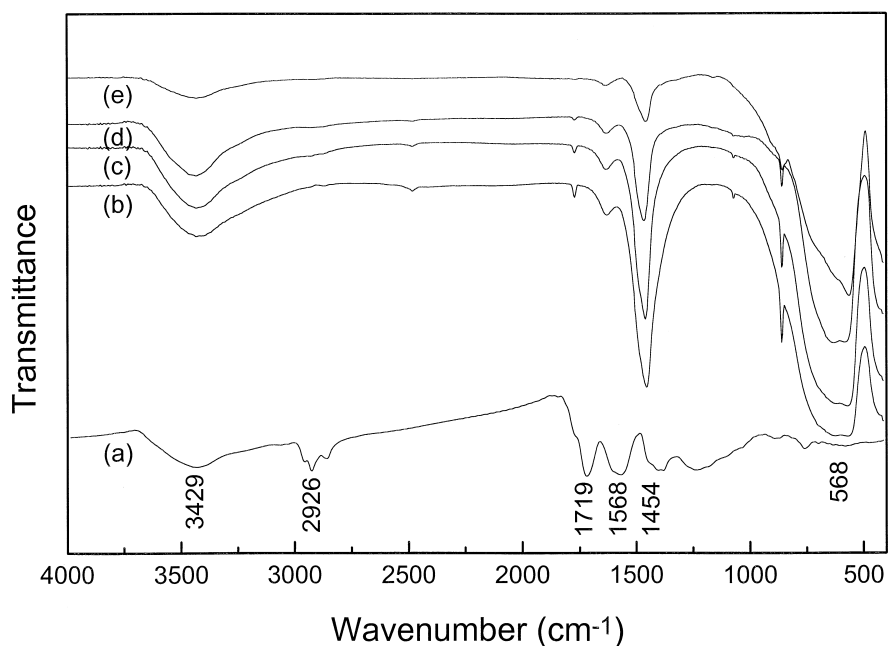

Fig. 4. Infra-red spectra of SrTiO$_3$:Al, Pr phosphors calcinated with different temperatures: (a) 350°C, (b) 600°C, (c) 800°C, (d) 1000°C, and (e) 1200°C.

results are supported by the shape of the nitrogen adsorption/desorption hysteresis curves for SrTiO$_3$ powders calcined at different temperatures (Fig. 7a). This figure shows an isotherm of type II[14] adsorption/desorption curve and a hysteresis H-1. It is indicated that the presence of mesopores (pores with a diameter of 2–100 nm) and open porosity with cylindrical geometry.[15] As can be seen from the figure, the shape of the curves for powders calcined at 600 and 900°C are very similar, however, the curve for the powder calcined at 1000°C has a different shape. Pore size distribution curves obtained by the BJH method (Fig. 7b) indicate

similar behavior with Fig. 7a. While the mean pore size changes from 23 nm at 600°C to 38 nm at 900°C, for powders that have been calcined at 1000°C, the total pore volume decreases dramatically and the shape of the pore size distribution changes significantly.

3.3. Luminescence properties

Fig. 8 shows the excitation spectra of four SrTiO$_3$ phosphors monitored at 617 and scanned from 200 to 550 nm. As can be seen from the figure, the excitation spectra are dependent on the Pr^{3+} or the Al^{3+}. These
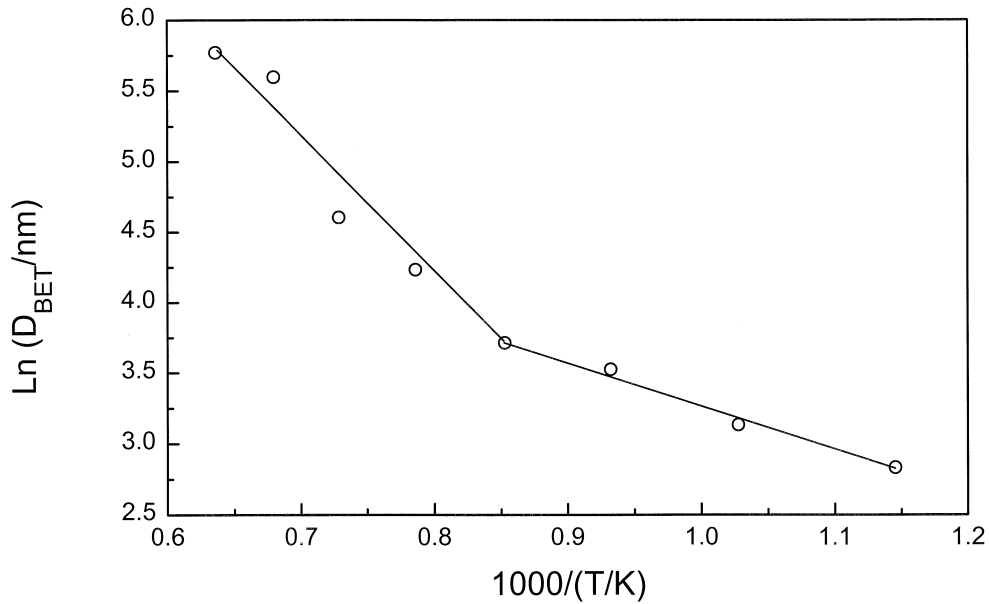
Fig. 5. Plot of Ln D_{BET} in $SrTiO_3$:Al, Pr phosphors as a function of $1/T$.
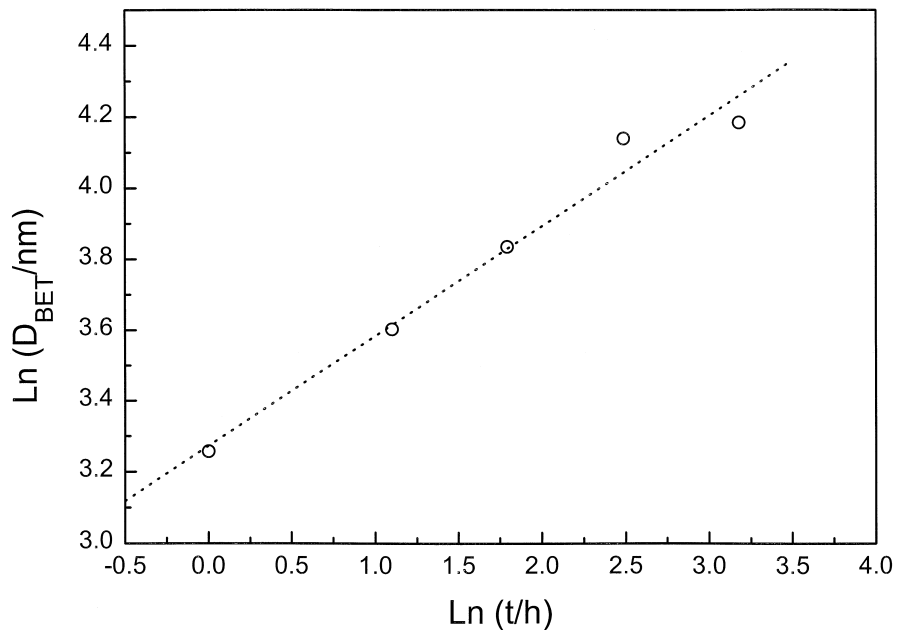
Fig. 6. Plot of Ln D_{BET} in $SrTiO_3$:Al, Pr phosphors as a function of Ln t for $SrTiO_3$:Al, Pr phosphor calcined with 1200°C.

phosphors exhibit a weak absorption band, but line (d) gives the optical absorption transitions. There are four excited peaks at 223, 243 and 359 nm in the excitation figure. Excited levels of Pr^{3+} ion are seen at 359 nm and the remaining peaks are excited levels of the Al^{3+} ion. The excitation spectrum for Pr^{3+} emission at 617 nm is the $^1S_0 \rightarrow {}^1D_2$ transition. An absorption edge is located at around 395 nm (25 000 cm^{-1}), and some peaks are detected at about 460 and 495 nm. This indicates that some peaks assigned to the transitions from the $^3H_4$ ground state to the $^3P_0 + {}^3P_1 + {}^1I_6 + {}^3P_2$ excited states are related to splitting of the 5d configuration.

Fig. 9 shows excitation spectra for Pr^{3+} emission at 617 nm with various delay times. All excitation spectra show the same pattern, independent of delay times. The effect of delay time is associated with nonradiative transitions. At long delay time, the excited states of atoms should be affected by interaction with neighboring atoms, caused by nonradiative transitions. For this reason, the longer the delay time, the smaller the absorption energy.

Fig. 10 shows photoluminescence emission spectra of $SrTiO_3$ with different Pr^{3+} concentrations. Under 359 nm excitation, $SrTiO_3$:Al, Pr phosphors exhibit a
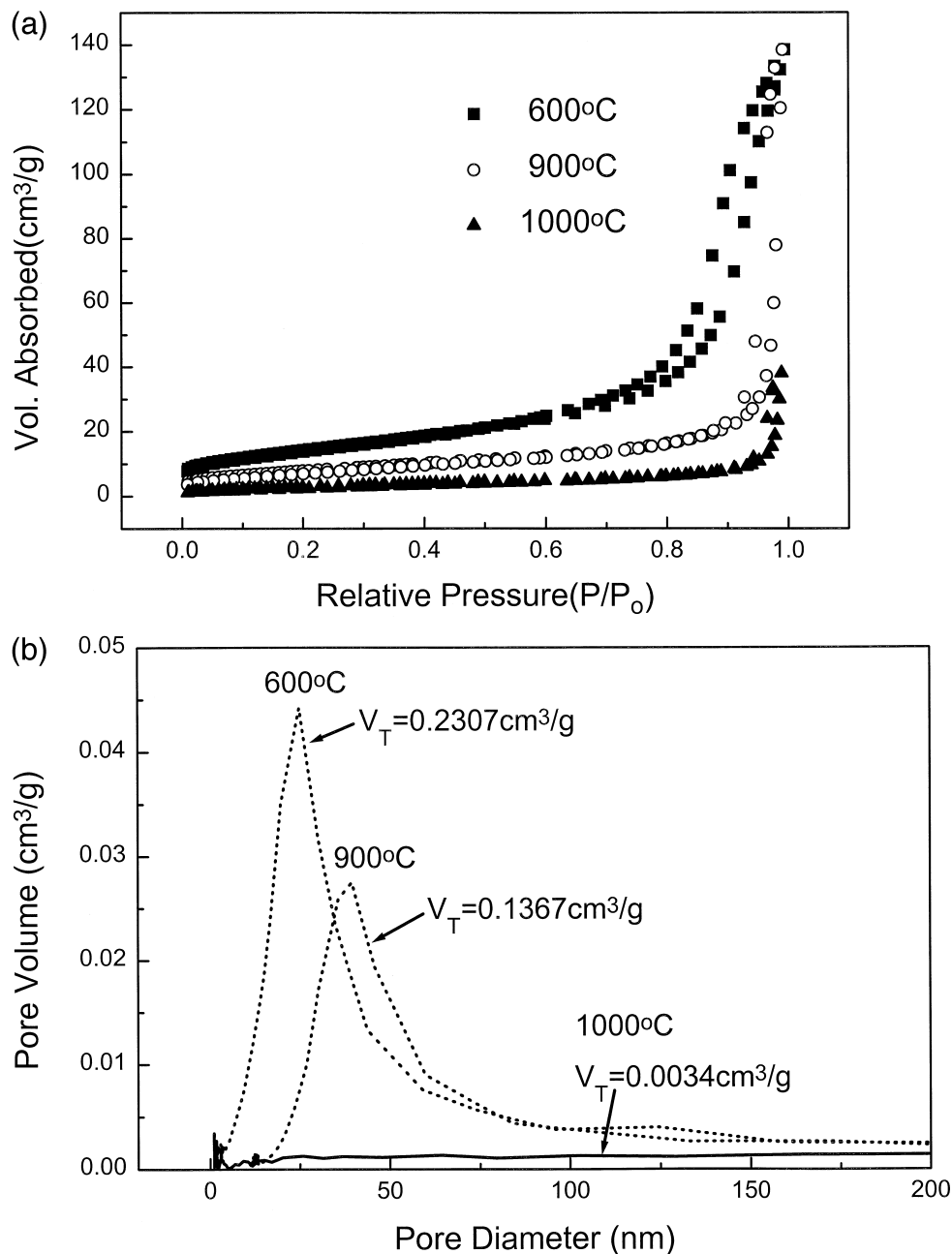
Fig. 7. (a) Adsorption/desorption hysteresis curves for SrTiO$_3$:Al, Pr phosphors calcined with different temperatures (b) pore size distribution curves obtained from desorption of nitrogen for SrTiO$_3$:Al, Pr phosphors calcined with different temperatures.

strong red emission due to the radiative $^1D_2 \rightarrow {}^3H_4$ transition. This agrees with the results of the emission color of Pr^{3+}.[16] Had the emission originated from the $^3P_0$ level, it would be green ($^3P_0 \rightarrow {}^3H_4$ transition) as in Gd_2O_2S:Pr; however, if the emission originated from the $^1D_2$ level, it would be red. Okumura et al.[17] have shown that the Pr^{3+} ion and the surrounding oxygen determine the emission level of Pr^{3+} in Y_2O_3. Based on their study, the shorter distance between the Pr^{3+} ion and oxygen causes a red emission ($^1D_2$ emitting level), while longer distance causes the green emission ($^3P_0$ emitting level). The critical distance at the Pr^{3+} for

emission state changes between $^3P_0$ and $^1D_2$ is about 0.24 nm. In this figure, $^3P_0$ emission is not under $^3H_4 \rightarrow {}^3P_J$ excitation, but under direct excitation of the $^1D_2$ state. For this reason, the emission is assumed to be radiative decay of the $^1D_2$ state ($^1D_2 \rightarrow {}^3H_4$ transition). The maximum emission intensity is at 0.2 mol% Pr^{3+} and the emission intensity decreases with increasing Pr^{3+} concentrations. Leverenz[18] has proposed an explanation of this concentration quenching phenomena. According to his results, optimum concentration of Mn in $ZnSiO_4$ is approximately 0.3 wt.%. At above 0.5 Mn wt.% in the host material, it is generally found that
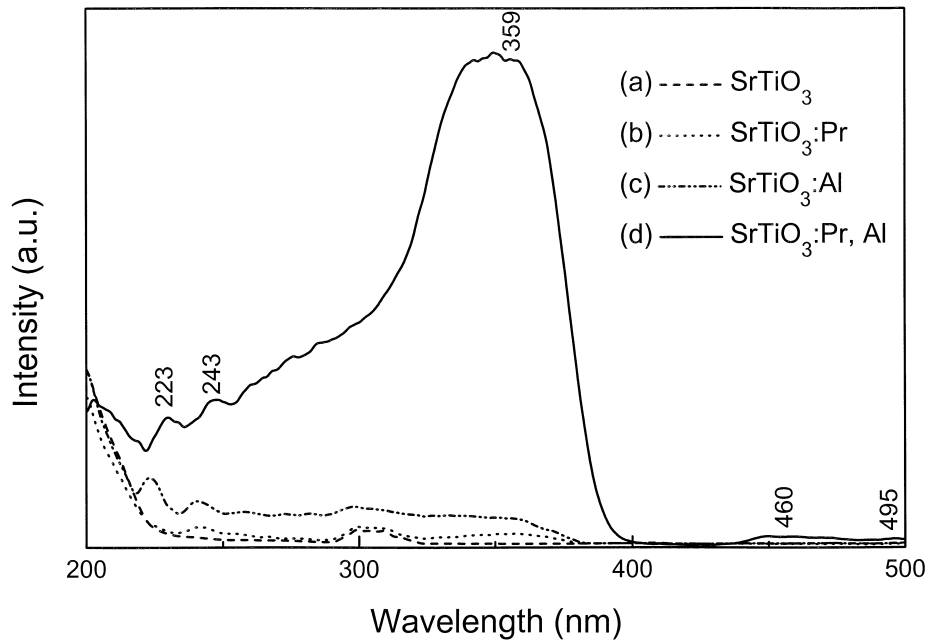
Fig. 8. Excitation spectra of (a) $SrTiO_3$, (b) $SrTiO_3$: Pr, (c) $SrTiO_3$:Al, and (d) $SrTiO_3$:Al, Pr monitored at 617 nm.
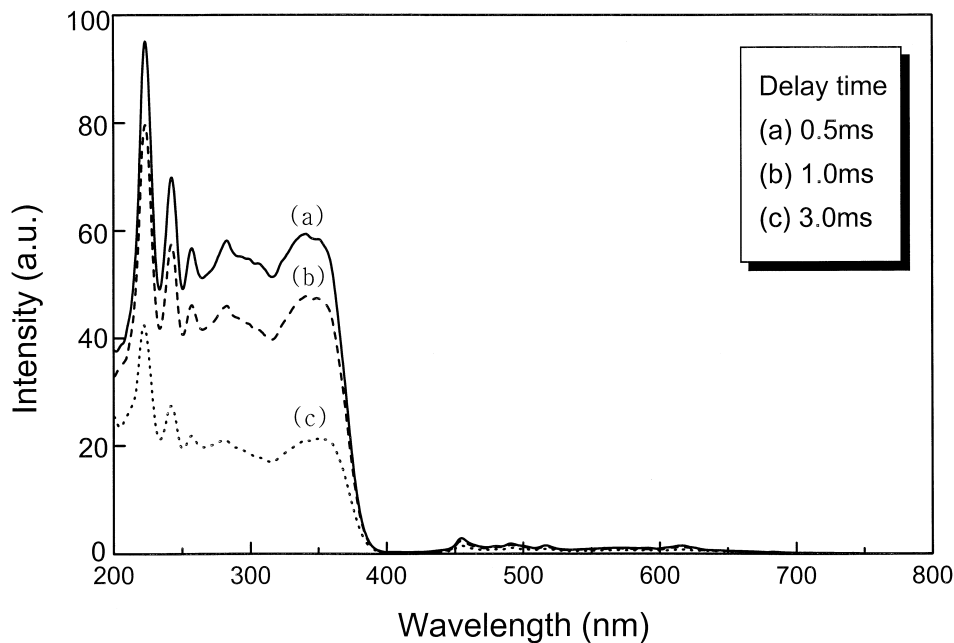

Fig. 9. Excitation spectra of the $SrTiO_3$:Al, Pr phosphors with various delay times.

increases in chemical complexity and structural heterogeneity of phosphors decreased their relative emission intensity. These phenomena may be attributed to concentration quenching, though the mechanism of concentration quenching is not yet clearly understood. As mentioned above, the change in critical distance at the Pr^{3+} emission state from $^3P_0$ to $^1D_2$ is about 0.24 nm.[17] As activator concentration increased, the oxygen vacancy formed at the nearest neighbor oxygens. Therefore, the distance between the Pr^{3+} ion and the surrounding oxygen may be shorter. This leads to enhanced strength of the electric–dipolar interaction between neighboring activator ions. Kuleshov et al.[19] reported that the luminescence quenching that was observed in crystals with different concentrations of Pr^{3+} is associated with intraionic nonradiative relaxation from the $^1D_2$ state to the lower $^1G_4$ state.

According to Dexter and Schulman,[20] concentration quenching is in many cases due to energy transfer from one activator to another, until an energy sink in the
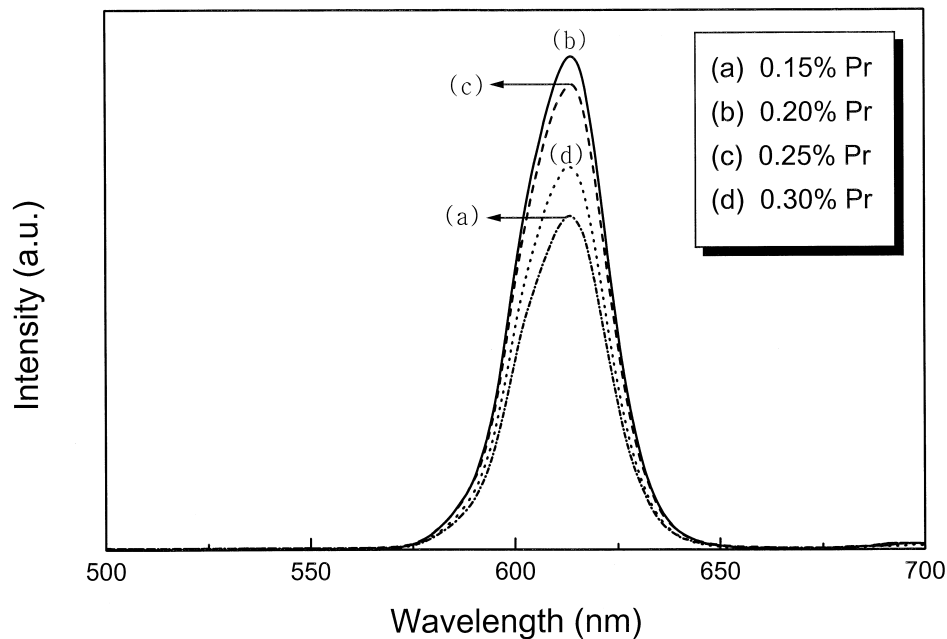
Fig. 10. Emission spectra of the $SrTiO_3$:Al, Pr phosphors under 359 nm excitation as function of Pr^{3+} contents.

lattice is reached. This suggests that concentration quenching is related to interaction between an activator and another sensitizer. This kind of interaction allows the absorbed excitation energy to reach particular quenching centers, so that the critical concentration depends on the probability of the transfer. For this reason, the critical concentration of concentration quenching can be used as a measure of the critical distance (R_C) of energy transfer. In the present case, where sensitizer and activator are identical, it is possible to obtain the values of R_C from the concentration quenching data.[21] The R_C values can be practically calculated using the following equation.

$$R_C = 2\left(\frac{3V}{4\pi x_C N}\right)^{1/3}$$

where x_c is critical concentration, N is the number of Al^{3+} ions and Pr^{3+} ions in the unit cell and V is the volume of the unit cell (in this case, the volume is 59.92Å^3).[22] The concentration quenching data for photoluminescence measurement with concentration of Pr^{3+} is shown in Fig. 10. In order to calculate the R_C and where the activator (Pr^{3+}) is substituted for a perovskite structure, we use the above equation. The calculated R_C value was 18 Å for substitution of Pr^{3+} at Sr sites and 38 Å for Ti sites. From these values, the critical distance (R_C) of energy transfer was larger than the distance (R) between the Al^{3+} ion and the Pr^{3+} ion; this is identical to the lattice parameter of $SrTiO_3$. As a result of the calculated critical distance, it is presumed that the energy transfer between the Al^{3+} and the Pr^{3+} ions is the governing factor in the case of the $SrTiO_3$:Al, Pr phosphor.

4. Conclusions

Using polymeric precursors, we prepared fine powders of $SrTiO_3$:Al, Pr red phosphors with little agglomeration. This method yielded $SrTiO_3$ formation at lower temperatures than required for conventional solid state reaction methods. The reason for this lowering of the reaction temperature might be associated with the low energy barriers of 59 KJ/mol for crystal growth at temperatures below 900°C (168 KJ/mol at higher temperatures).

The $SrTiO_3$:Al, Pr phosphor has a red emission band between 575 and 650 nm peaking at 617 nm. This is due to the radiative decay of the $^1D_2$ states ($^1D_2 \rightarrow {}^3H_4$ transition). Emission intensity increased with increasing activator concentration up to a maximum at 0.2 mol% Pr^{3+} ions. Beyond this doping level, emission intensity decreased with increasing Pr^{3+} contents, presumably due to concentration quenching. The critical distance (R_C) for energy transfer calculated from these concentration quenching data indicates, that in $SrTiO_3$:Al, Pr phosphors the energy transfer between Al^{3+} and Pr^{3+} is the governing factor.

References

1. Kang, Y. C., Choi, J. S., Park, S. B., Cho, S. H., Yoo, J. S. and Lee, J. D., Preparation of spherical YAG:Tb phosphor by spray pyrolysis using filter expansion aerosol generator. *Extended Abstracts of the Third International Conference on the Science and Technology of Display of Phosphors*, 1997, 3–5 November, pp. 257–260.
2. Vogel, E. M., Andreadakis, N. C., Quinn, W. E. and Nelson, T. J., Materials for display devices based on metallo–organic precursors. Ceramic powder science, *The American Ceramic Society*, 1987, **21**, 131–137.

3. Brownlow, T. M. and Chang, I. F., Novel synthesis technique for zinc-silicate phosphors. *IEEE Trans. Elec. Devices*, 1983, **ED-30**(5), 479–483.

4. Pechini, M. P., Preparation of strontium titanate ceramic and internal boundary layer capacitors by the pechini method. US Patent 3330697, 11 July 1967.

5. Error, N. G. and Anderson, H. V., Polymeric precursor synthesis of ceramic materials. *Mater. Res. Soc. Symp. Proc.*, 1986, **73**, 571–578.

6. Park, J. K., Ryu, H., Kim, K. H. and Park, H. D., Observation of energy transfer between Al^{3+} and Pr^{3+} in $SrTiO_3$ phosphor. *Electrochem. Solid State Lett.*, 2000, **3**(2), 110–112.

7. Cullity, B. D., *Elements of X-Ray Diffraction*, 2nd edn. Addison-Wesley, Reading, MA, 1978 pp. 96–103.

8. Cerqveira, M., Nasar, R. S. and Longo, E., Synthesis of ultra-fine crystalline $Zr_xTi_{1-x}O_4$ powder by polymeric precursor method. *Mater. Lett.*, 1995, **22**, 181–185.

9. Last, J. T., Infrared absorption studies on barium titanate and related materials. *Phys. Rev.*, 1957, **105**(6), 1740–1750.

10. Gülgün, M. A., Popoola, O. O. and Kriven, W. M., Chemical synthesis and characterization of calcium aluminate powders. *J. Am. Ceram. Soc.*, 1994, **77**(2), 531–539.

11. Brook, R. J., Controlled grain growth. *Ceram. Fabric. Proc.*, 1976, **9**, 331–364.

12. Glacsar, A. M., Microstructure development in ceramics: the role of grain growth. *Yogyo Kyokaishi*, 1984, **92**(10), 537–546.

13. Greskovich, C. and Lay, K. W., Grain growth in very porous Al_2O_3 compacts. *J. Am. Cerm. Soc.*, 1972, **55**(3), 142–146.

14. Brunauer, S., Deming, L. S., Deming, W. E. and Teller, E., On a theory of the Van der Walls adsorption of gases. *J. Am. Chem. Soc.*, 1940, **62**, 1723–1732.

15. Sing, K. S. W., Reporting physisorption data for gas/solid systems with special reference to the determination of surface area and porosity. *Pure Appl. Chem.*, 1982, **54**(11), 2201–2218.

16. Blasse, G. and Grabmaier, B. C., *Luminescent Materials*. Springer, Berlin, 1994, p. 45.

17. Okumura, M., Tamatani, M., Albessard, A. K. and Matosuda, N., Luminescence properties of rare earth ion-doped monoclinic yttrium sesquioxide. *Jpn. J. Appl. Phys.*, 1977, **36**, 6411–6415.

18. Leverenz, H. W., *An Introduction to Luminescence of Solids*. Dover, New York, 1968, p. 336.

19. Kuleshov, N. V., Shcherbitsky, V. G., Lagatsky, A. A., Mikhailov, V. P., Minkov, B. I., Danger, T., Sandrock, T. and Huber, G., Spectroscopy and excited-state absorption of Ni^{2+}-doped $MgAl_2O_4$. *J. Lumin.*, 1997, **71**, 27–35.

20. Dexter, D. L. and Schulman, J. A., Theory of concentration quenching in inorganic phosphors. *J. Chem. Phys.*, 1954, **V22**(N6), 1063–1070.

21. Blasse, G., Energy transfer in oxidic phosphors. *Philips Res. Repts.*, 1969, **24**, 131–144.

22. Maslen, E. N., Spadaccini, N., Ito, I., Marumo, F. and Satow, Y., A synchrotron study of strontium titanate. *Acta Cryst*, 1995, **B51**, 939–942.